Progress In Electromagnetics Research C, Vol. 131, 259–273, 2023

Analysis and Design of Dual-Wide Band (28/38 GHz) Chebyshev Linear Antenna Array Integrated with 3D Printed Radome for 5G Applications

Ahmed Khairy[1, 3, *], Ayman Elboushi[2], Abdel A. Shaalan[3], and Mai F. Ahmed[3]

Abstract—This research presents the design of a Chebyshev linear antenna array (CLA) integrated with dielectric lens. In comparison to a uniform amplitude distribution (UAD), a Chebyshev amplitude distribution (CAD) is used to achieve a low side lobe level (SLL) characteristic and increase the directivity of the antenna array. The proposed CLA is optimized to operate at a high fifth generation (5G) frequency. The proposed CLA achieves a −10 dB wide bandwidth from 25.8 GHz to 42.4 GHz. Dielectric lenses can be employed to modify the phase and amplitude of the antenna array, which increases the realized gain and leads to stable radiation over the operational bandwidth. The main purposes of the dielectric lens are to improve the realized gain, enhance efficiency, and result in stable radiation pattern properties. Also, the research presents a study of two types of dielectric lenses with different shapes and their effects on the efficiency and the realized gain of the antenna. The substrate of the dielectric lens is epoxy resin, which has a relative permittivity (ε_r) of 2.716. The proposed CLA integrated with the proposed Type 2 dielectric lens has a realized gain of 15.2 dB and 11.94 dB at the dual-bands 28 GHz and 38 GHz, respectively. All the suggested designs are simulated using CSTMWS2020 and HFSS. However, to verify the obtained results, the proposed CLA is fabricated using a photolithography process technique, and the proposed Type 2 dielectric lens is fabricated using a 3D printing technique.

1. INTRODUCTION

Operation at high frequencies is a solution to achieve broadband and a high data transfer rate. Because the fourth generation (4G) suffers from congested spectrum and high power consumption, the fifth generation (5G) is a promising candidate for a wide spectrum that supports high data transfer rates required for various applications such as streaming services and automotive applications. The proposed design is an mm-wave antenna array, which is optimized to operate at 28 GHz and 38 GHz with wideband characteristics to be integrated with 5G automotive applications. The automotive applications cover some essential services including vehicle-to-vehicle (V2V), vehicle-to-everything (V2X), vehicle-to-pedestrian (V2P), wireless health care service, etc. [1, 2]. The mentioned services need an optional antenna, which has some properties such as wide bandwidth, high realized gain, and efficiency to work professionally in different critical environmental conditions and cover all different 5G services [3, 4]. Over recent years, dielectric lenses have received great interest, especially for mm-wave antennas, to have a suitable size and an easier fabrication process because of their great impact on the realized gain of the antenna as well as beamforming technique. These linear array antennas are commonly used in wireless communications and automotive applications because of their high gain, small weight, low cost, and low

Received 3 February 2023, Accepted 27 March 2023, Scheduled 3 April 2023
* Corresponding author: Ahmed Khairy (Ahmed.khairy@eaeat.edu.eg).
[1] Egyptian Academy for Engineering and Advanced Technology, Cairo, Egypt. [2] Microstrip Department, Electronics Research Institute, Nozha, Egypt. [3] Department of Electronics and Communications Engineering, Faculty of Engineering, Zagazig University, Zagazig, Egypt.

profile, as well as the ability to control radiation patterns [5]. The dielectric lenses are used to modify the main radiation pattern into a high gain radiation pattern for fixed or beamforming services [6]. The proposed Chebyshev linear array (CLA) is integrated with a dielectric lens, which is optimized by using two different software packages, and to verify the simulated results, the proposed design is fabricated. The CAD is used to reduce SLL. The CAD can be applied by changing the dimension of patch elements of the array, which leads to a change in the amplitude of a single element in the proposed array. Chebyshev polynomial array antennas produce the best amplitude distribution in which all side lobe levels (SLLs) are identical to the desired level by using equal-power Dolph-Chebyshev polynomials to match the Fourier polynomial. It gains from the property that, although R (SLL) achieves its maximum value at a certain beam width, the beam width at the first zero is the smallest at a specific ratio R. The Dolph-Chebyshev polynomial is typically used to construct array antennas because of this property [7]. In millimeter-wave applications, dielectric lens antennas are gaining popularity, particularly in designs with integrated feeds, which are often referred to as "integrated lens antennas." Lenses are a dependable substitute for reflector antennas at these frequencies because they are incredibly flexible and easy to design and manufacture. The output of a lens might be anything from a straightforward collimated beam to more intricate multi-objective specs [8]. There are several ways to create a dielectric lens antenna. The most typical methods either make use of computer numerical control (CNC), molding, or 3D printing. Through the use of CNC technology, real items may be created from their digital 3D descriptions by autonomously extracting their shape from a block of raw materials. The shaped lens antennas operate at millimeter waves; this sort of manufacturing technique is especially suitable for lenses with complicated forms, close dimensional tolerances, and excellent surface smoothness. In contrast to, for instance, the injection molding method, which is cost-effective for mass production, it is more appropriate for small series manufacturing or lab prototyping. However, the latter technology may enable the use of CNC for mold fabrication for dielectric lenses [8]. High-quality materials that adhere to strict criteria are required to create reliable, high-quality products using 3D printing. Procedures, demands, and agreements about material controls are developed between the suppliers, buyers, and end-users of the material in order to achieve this. Using a variety of materials, such as ceramics, metals, polymers, and their mixtures to create hybrid, composite, or functionally graded materials, 3D printing technology may create completely functioning components [9]. Additionally, photo polymerization, which generally refers to the curing of photo reactive polymers using a laser, light, or ultraviolet (UV) radiation [10], is the primary 3D printing technology that is widely employed. The photo initiator and irradiate exposure settings, as well as any additional UV absorbers like dyes or pigments, had an impact on the SLA [11]. Digital light processing (DLP), on the other hand, uses photopolymers in a manner that is comparable to stereo lithography [12]. When the liquid is subjected to UV radiation, the components that were previously employed as liquids will harden. A premium product with excellent details and a high-quality surface may be produced using photo polymerization [9].

2. ANTENNA ARRAY ELEMENTS DESIGN

The proposed CLA is optimized to introduce wideband, high realized gain, and low SLL by using CAD in antenna array element design [13]. In addition, the proposed design has taken into consideration all patch dimensions, which are designed to resonate at 28 GHz and 38 GHz with wide broadband characteristics to cover the high 5G frequency band. However, a uniform linear array (ULA) is designed to show the essential difference between ULA and CLA. The two proposed antennas CLA and ULA are designed using Roger RT5880, which has a relative permittivity of ($\varepsilon_r = 2.2$). The thickness of the substrate is 0.7874 mm and has tangent losses ($\tan\delta = 0.0009$). The proposed CLA and ULA factors are shown in Figure 1. For an even number of elements, the CLA factor of the series array can be written as [14]:

$$(\mathrm{AF}) = \sum_{n=1}^{4} a_n \cos\left(2n-1\right)\Psi \tag{1}$$

$$\Psi = Kd\cos(\theta) \tag{2}$$

The four-unit Chebyshev polynomial is defined by the Chebyshev general theoretical formula as:

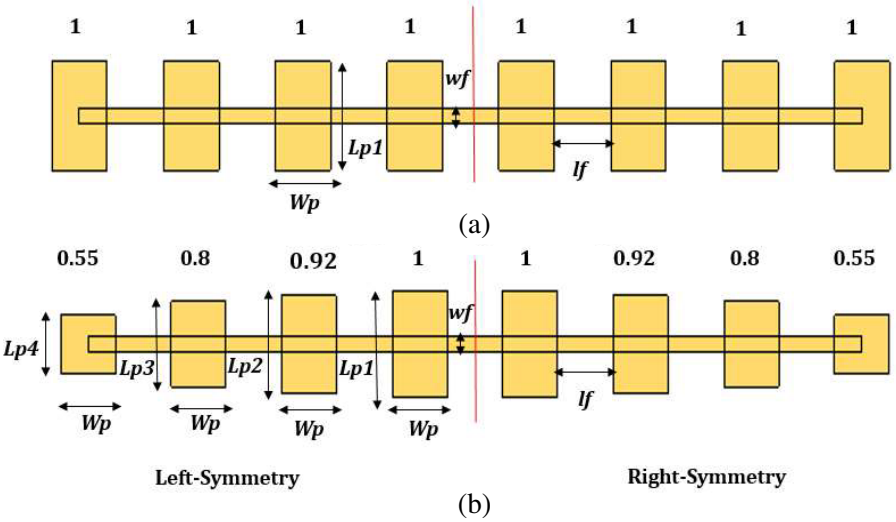

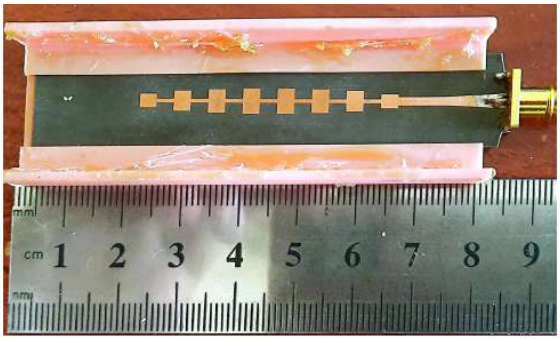

Figure 1. The geometry and element factors of the ULA and CLA. (a) ULA proposed design. (b) CLA proposed design.

$$T_4(z) = 8Z^4 - 8Z^2 + 1 \tag{3}$$

where $T_m(z)$ is a Tschebyscheff (Chebyshev) polynomial and $z = \cos(mu)$, $-1 \leq z \leq 1$.

The electric field of 4 unit elements in vertical direction is:

$$En_4 = 2 \sum_{k=0}^{K=N-1} a_k \cos\left[(2k+1)\frac{\pi d \sin\theta}{\lambda}\right] \tag{4}$$

Table 1. The optimized dimensions of the proposed ULA and CLA.

parameter	Value (mm)	λ_o	λ_g
Wp	2.9	0.3193	0.4738
$Lp1$	4.38	0.4823	0.7156
$Lp2$	4.03	0.4438	0.6584
$Lp3$	3.50	0.3854	0.5718
$Lp4$	2.41	0.26541	0.3937
Wf	0.7	0.07709	0.1143
Lf	2.95	0.32488	0.4820

The side lobe level can be defined as:

$$Z_o = \frac{1}{2}\left[\left(R_0 + \sqrt{R_0^2 - 1}\right)^{\frac{1}{N-1}} + \left(R_0 - \sqrt{R_0^2 - 1}\right)^{\frac{1}{N-1}}\right] \quad (5)$$

where R_0 is the SLL, and N represents the number of array elements.

The dimensions of the proposed CLA and ULA are presented in Table 1. The dimensions of the proposed CLA are obtained by using a parametric study in CSTMWS 2020.

The return loss $|S_{11}|$ of ULA and CLA is simulated by using CSTMWS 2020 and HFSS. Also, the CLA is fabricated, and S_{11} is measured as shown in Figure 2.

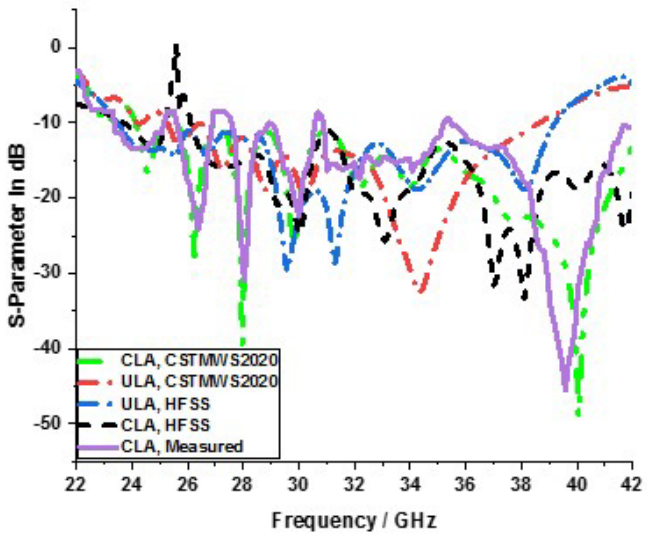

Figure 2. The return loss $|S_{11}|$ of CLA and ULA.

The return loss $|S_{11}|$ of CLA shows a -10 dB wide bandwidth from 24 GHz to 40.5 GHz.

The radiation patterns of the proposed antenna are measured at 28 and 38 GHz. Also, the maximum gain versus frequency is measured and presented in Figure 13. The experimental setup is presented in Figure 3. The VNA Rhode and Schwartz model ZVA67 is set to operate in the two-port measurement mode for the purpose of measuring the transmission coefficient $|S_{21}|$ through the antenna under test (port 1) and the reference-gain antenna (port 2). LB-018400 is a reference gain antenna which is linearly-polarized horn employed in the measurements. The separation between the two antennas is 40 cm. The radiation patterns in the elevation $\phi = 0°$ and azimuth $\theta = 90°$ planes are measured for the proposed antenna. The radiation patterns for the CLA and the CLA integrated with the proposed Type 2 dielectric lens are presented in Figure 4 and Figure 12 at the frequencies of 28 GHz and 38 GHz respectively.

Figure 3. The experimental setup for the measured radiation pattern and realized gain.

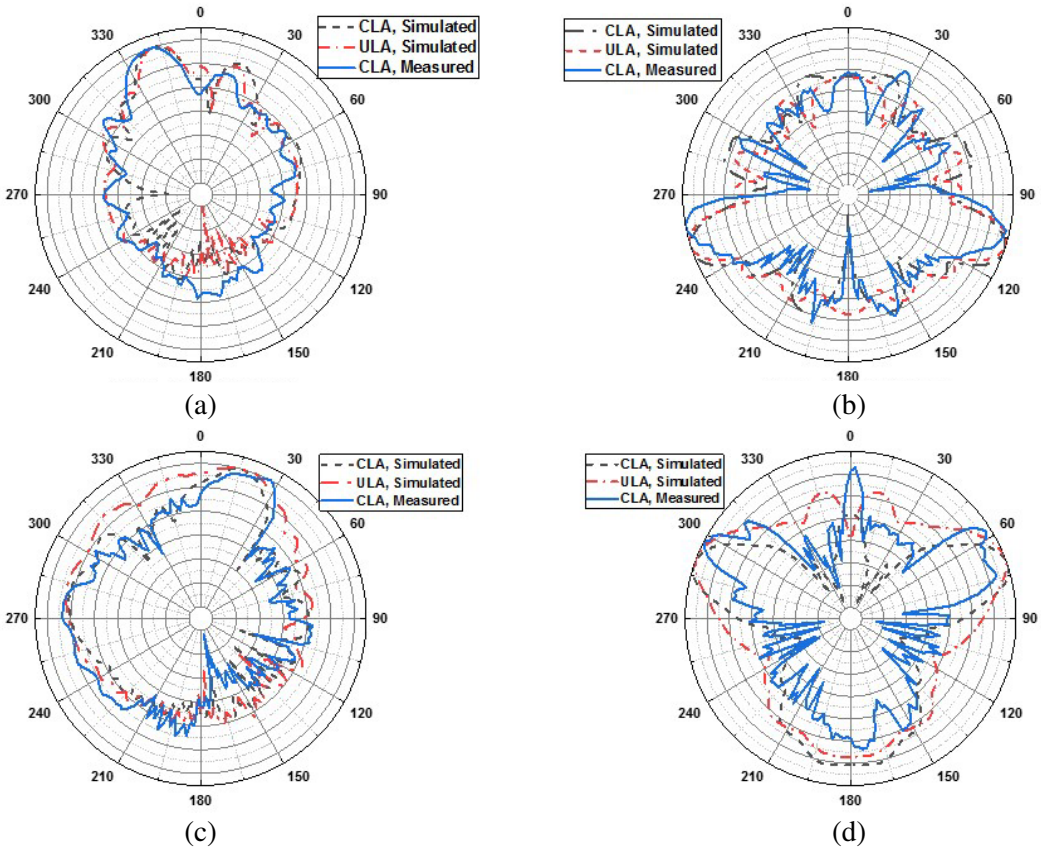

Figure 4. The 2D normalized radiation patterns of the CLA and the ULA. (a) E-plane (28 GHz), (b) H-plane (28 GHz), (c) E-plane (38 GHz), (d) H-plane (38 GHz).

Several designs have been introduced to reduce SLL, enhance bandwidth, and increase realized gain. To compare the UAD and CAD linear arrays, the ULA and CLA were designed and optimized mainly to operate at 5G high-frequency bands including 28 GHz and 38 GHz by using CSTMWS 2020 and HFSS. The comparison between the CLA and ULA is presented in Table 2. The realized gain of proposed CLA and ULA is shown in Figure 13. The simulated total efficiency using CSTMWS 2020 is shown in Figure 14. Also, Figure 4 shows the 2D radiation patterns of the CLA and the ULA.

Table 2. Compares the CLA and the ULA in 5G high frequency bands.

linear antenna array (type)	CLA	ULA
Impedance bandwidth	49.58%	41.92%
MaxRealized gain at 28 GHz	14.4 dB	14.2 dB
MaxRealized gain at 38 GHz	11.3 dB	9.4 dB
SLL at 28 GHz	−9 dB	−9.2 dB
SLL at 38 GHz	−8.5 dB	−4.6 dB
Total Efficiency at 28 GHz	91%	89%
Total Efficiency at 38 GHz	93%	88%
Angular width (3 dB) at 28 GHz	12.8°	11.7°
Angular width (3 dB) at 38 GHz	14.2°	26.3°

Because of the CAD in the proposed CLA, the CLA has a more confined radiation pattern and a lower SLL than the ULA.

From the previous comparison, the CLA antenna gives better results than the ULA antenna in terms of realized gain, SLL, impedance bandwidth, efficiency, and half-power beam width (HPBW).

3. CLA WITH DIELECTRIC SUPERSTRATE (DS)

The DS is designed to increase the directivity of the radiated beam by collimating incident rays from air to the dielectric plane of the lens [15]. The DS operates much like an optical lens according to Snell's law. The principle of operation is a collimated incident electromagnetic wave from the air, whose ($\varepsilon_r = 1$) to the lens plane has a high ($\varepsilon_r = 2.716$) [16]. The incidence wave that passes through the DS is collimated because of the refraction process [17]. The dielectric material used in the proposed design is epoxy resin, whose $\varepsilon_r = 2.716$ [18, 19]. The principle of operation is shown in Figure 5.

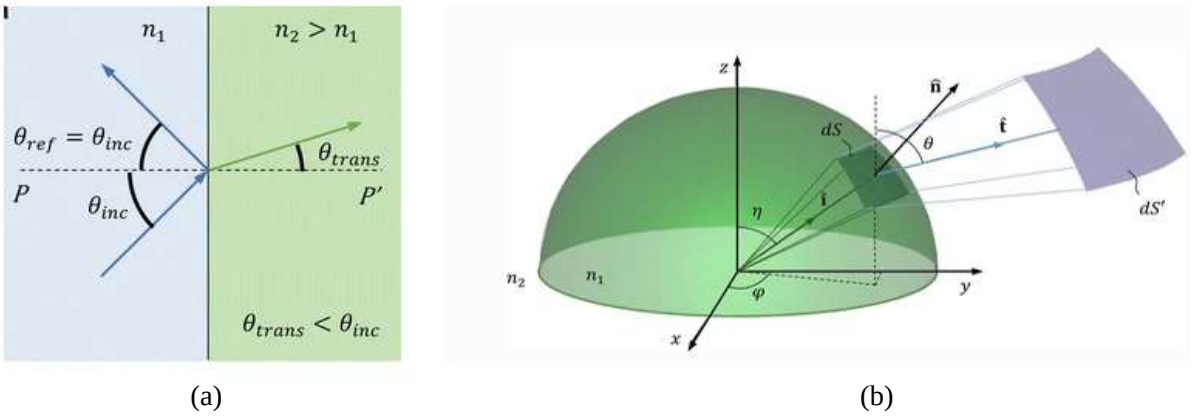

Figure 5. (a) Incidence wave from the lower to high index medium. (b) Geometry of dielectric lens [17].

The equations that describe the refraction process and principle of a collimating beam in a dielectric lens are [8, 20]:

$$\sqrt{\varepsilon_{r1}}\sin(\theta_{\text{inc}}) = \sqrt{\varepsilon_{r2}}\sin(\theta_{\text{trans}}) \tag{6}$$

where θ_{inc} and θ_{trans} are the incident and transmission angles with respect to the normal interface, and ε_{r1} and ε_{r2} are the relative electric permittivity of each medium.

$$\left(n_1\hat{i} - n_2\hat{t}\right) x\hat{n} = 0 \tag{7}$$

where n_1 and n_2 are the refraction indexes of each medium; $\hat{i}$ and $\hat{t}$ represent the incident and refracted wave number vectors, respectively as shown in Figure 5. $\hat{n}$ represents the normal surface vector.

$$\frac{dr}{d\eta} = \frac{\sqrt{\varepsilon_{r2}}r\sin(\theta-\eta)}{\left(\sqrt{\varepsilon_{r1}} - \sqrt{\varepsilon_{r2}}\right)\cos(\theta-\eta)} \tag{8}$$

where n_1 and n_2 are the refractive indexes of each medium. The output angle function $\theta(\eta)$ is the other unknown, and it will be determined by some design constraint involving phase, amplitude, or eventually polarization. $r(\eta)$ represents the unknown dielectric lens profile. A differential equation or an algebraic equation might both meet this requirement. With the appropriate beginning conditions $r(0)$ and $\eta(0)$ and a final value of max, the simultaneous equations must be integrated in the range $\eta \in [0, \eta_{\max}]$ [8]. The final lens shape is quickly produced by numerically doing this integration, which is often done [8]. The epoxy resin is used in 3D printing to fabricate the proposed lens. The DS is optimized to operate in a 5G high-frequency band to integrate with the CLA antenna, as shown in Figure 6. The optimized dimensions of the proposed DS are optimized and obtained in Table 3.

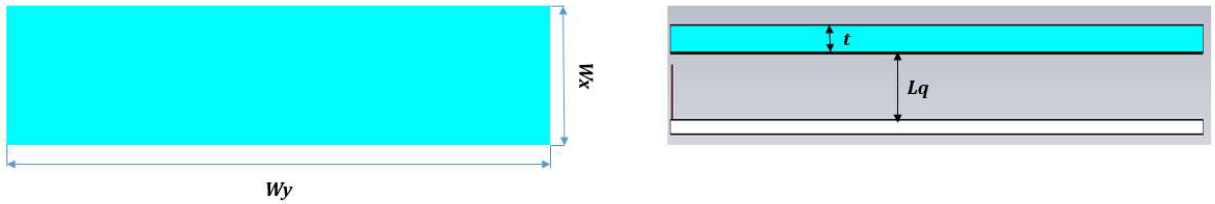

Figure 6. (a) The top-view of the dielectric superstrate and (b) the front-view of the CLA with dielectric superstrate.

Table 3. The optimized dimensions of the proposed dielectric superstrate.

parameter	Wx	Wy	Lq	t
Value (mm)	15	80	3.82	1.6

The return loss $|S_{11}|$ of CLA with DS is simulated by using CSTMWS2020 and HFSS as shown in Figure 7. Because the DS is mainly intended to promote the CLA gain, Figure 13 shows the achieved gain versus frequency for the proposed DS design. Also, the total efficiency is enhanced over the CLA and ULA as shown in Figure 14. The total efficiencies of CLA integrated with DS are 8743 and 93.87 at the operating frequencies of 28 GHz and 38 GHz, respectively.

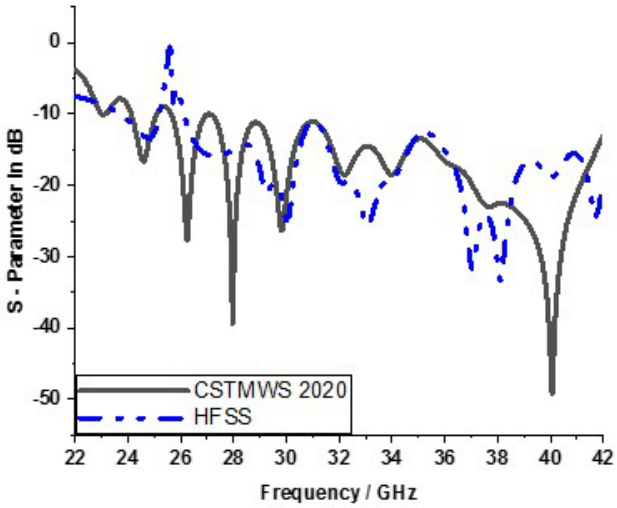

Figure 7. The return loss $|S_{11}|$ of the dielectric superstrate.

4. CLA INTEGRATED WITH DIELECTRIC LENS (SPECIAL DS)

The dielectric lens is a special case of DS, which is designed to collimate incident wave that falls on the surface with high efficiency [21, 22]. In this part, a parametric study using CSTMWS2020 is carried out to verify the properties of some different surfaces of the dielectric lens made of resin. These characteristics are the ability of the dielectric lens collecting incident waves well to improve the gain, radiation efficiency and overall efficiency of the proposed CLA. Type 1 of the dielectric lens shape is illustrated in Figure 8. The optimized dimensions are obtained in Table 4.

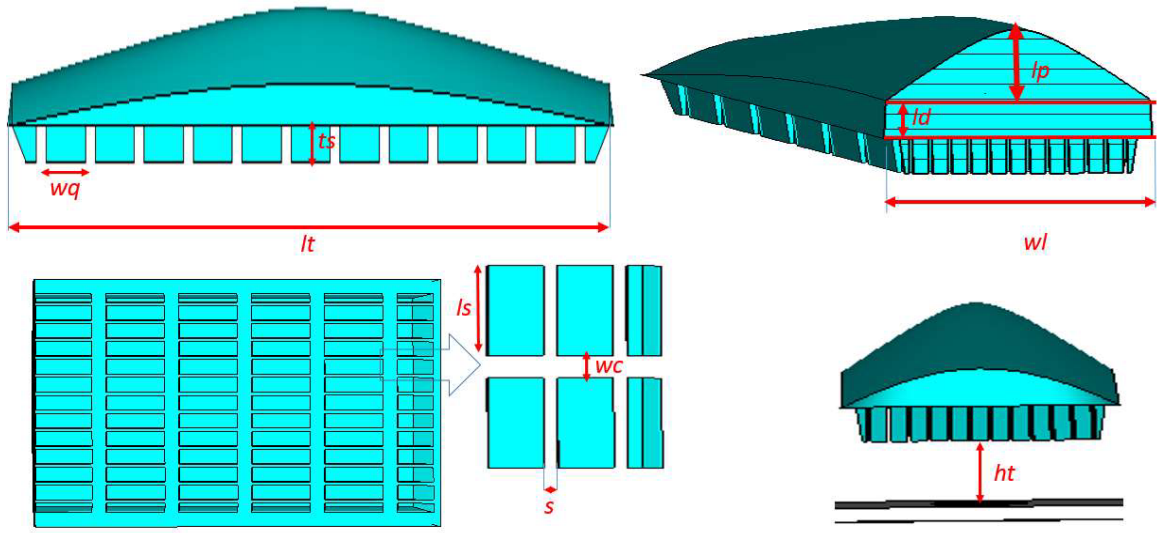

Figure 8. The first suggested form of the dielectric lens (Type 1).

Table 4. The optimized dimensions of the first suggested form of the dielectric lens.

parameter	wl	lt	ld	lp	wq	ts	ls	wc	ht	s
Value (mm)	19.8	79.5	2.18	8	0.72	2.02	5.28	1.32	3.8	0.18

The lens has a parabolic top surface and an array of a cubic shape in the bottom of the dielectric lens, and there is a small space between them as shown in Figure 8.

The return loss $|S_{11}|$ of Type 1 suggested form of the dielectric lens is shown in Figure 9. Also, the realized gain versus frequency is shown in Figure 13. The simulated total efficiency using CSTMWS 2020 is shown in Figure 14. Also, the total efficiency shows the difference between the suggested designs of the dielectric lenses.

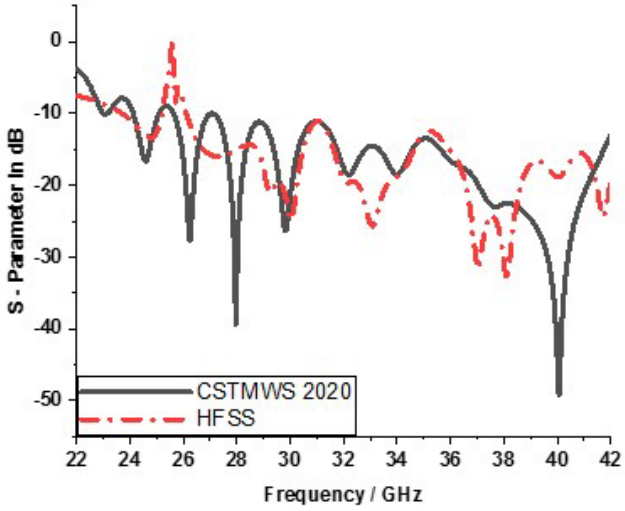

Figure 9. The return loss $|S_{11}|$ of the first suggested form of the dielectric lens (Type 1).

Table 5. The optimized dimensions of the second proposed dielectric lens.

parameter	L	W	Lq	Ld	lc	Lf	Lm	Ln	Wg	g
Value (mm)	79.5	19.8	3.8	5	2.02	8	5.15	1.4	1.3	0.5

Also, the second proposed dielectric lens has a top surface of parabolic shape with elliptical air cavities, as shown in Figure 10. The dimensions of the proposed dielectric lens are optimized and shown in Table 5. The proposed dielectric lens is fabricated using 3D printing technology. The material used in 3D printing is epoxy resin, which has a relative permittivity ε_r of 2.716. The total efficiencies of CLA integrated with the Type 1 proposed dielectric lens are 0.90 and 0.093 at the operating dual-band frequencies of 28 GHz and 38 GHz, respectively.

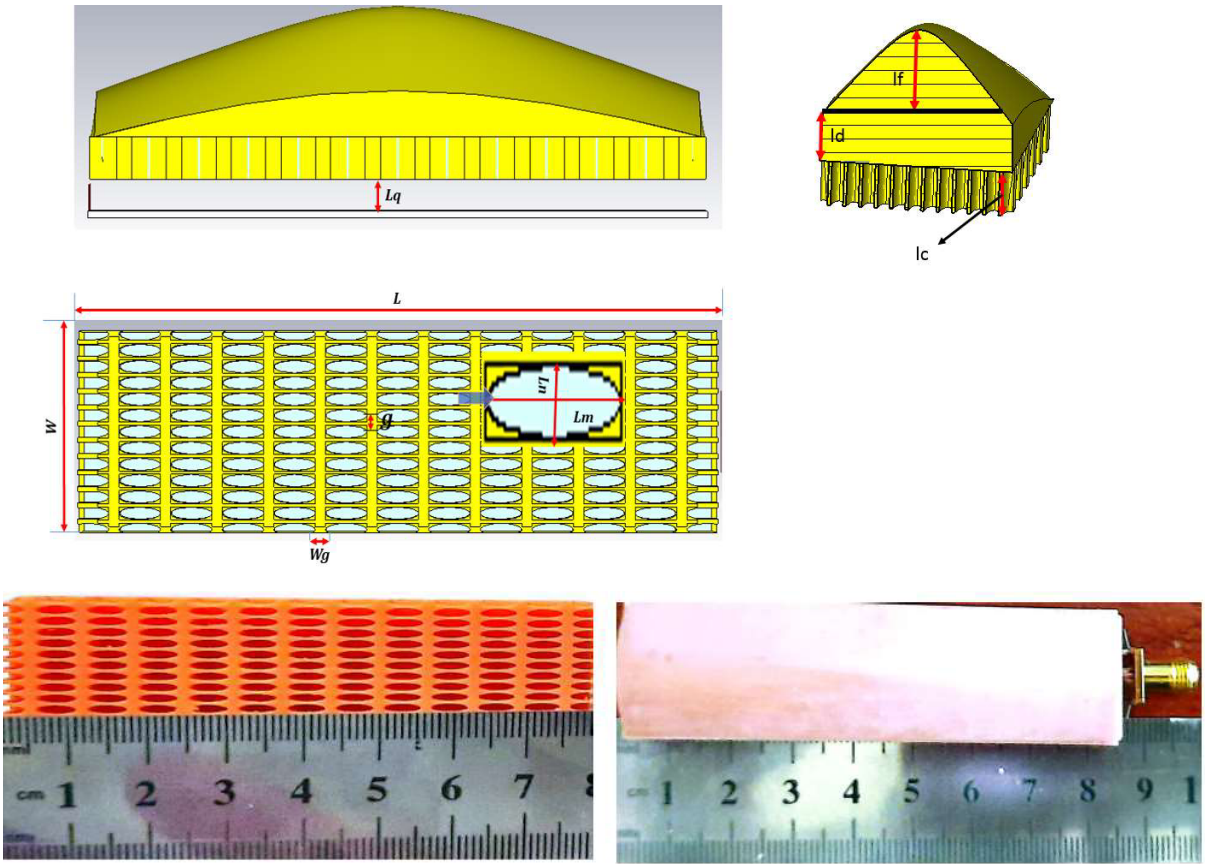

Figure 10. The second proposed dielectric lens design (Type 2).

3D printing is a technology in which epoxy resin is dropped drop by drop onto a building substrate and deposited selectively [23]. The printer discharges droplets of a photosensitive substance that solidify, layer by layer, forming a component under ultraviolet light. The material being jetted produces products with a highly smooth surface finish and high dimensional accuracy at the same time [9, 24]. The proposed dielectric length is fabricated with a smooth surface and high dimension accuracy [25]. 3D printing technology is now being employed in many sectors for quick and affordable prototype methods thanks to advancements in the industry and drops in prices. Because of its accurate, quick, and affordable prototype capabilities, 3D printing technology has recently been applied in various technical applications, particularly those using microwaves. Particularly in the prototyping of microwave antennas, 3D printers are often used to create models with complex structures or models that are impractical to prototype using conventional methods [26].

The proposed CLA antenna is integrated with the second proposed dielectric lens (Type 2) to enhance its performance. The return loss $|S_{11}|$ of a simulated and fabricated design is shown in Figure 11.

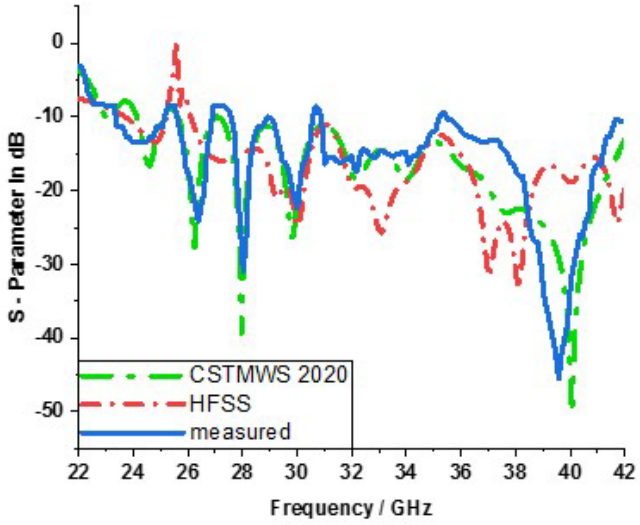

Figure 11. The return loss $|S_{11}|$ of the second proposed CLA integrated with dielectric lens (Type 2).

The dielectric material (dielectric lens) has no effect on the return loss of the proposed CLA antenna [8]. Also, the dielectric lens results in a confined, 9, pattern and high directivity, so the realized gain is increased, and the SLL is decreased [27]. The radiation patterns for the CLA and the CLA integrated with the Type 2 proposed dielectric lens are shown in Figure 12. The comparison between the proposed CLA integrated with the second dielectric lens and previous literature is presented in Table 6. In this comparison, the focus was on the characteristics of antennas that operate in the dual-frequency band (28/38 GHz). Recent literature mentioned in Table 6 has different characteristics to show the advantages of the proposed design. The CLA integrated with a dielectric lens (Type 2) is fabricated using 3D printing and has good properties such as a compact size, high gain, wide band at dual-band (28/38 GHz), and high efficiencies.

Table 6. Comparison between the CLA integrated with a dielectric lens and previous work at the same resonant frequencies.

Reference No	Resonant frequency (GHz)	Total Efficiency (%)	Bandwidth (GHz)	Gain (dB)
[28]	28 and 38	-	0.45 and 2.2	5.2 and 5.9
[29]	28 and 38	69	3.34 and 1.395	3.75 and 5.06
[30]	28 and 38	84	0.85 and 0.75	4 and 4.5
[31]	28 and 38	80	2.83 and 7.92	peak 4.63
[32]	28 and 38	96 and 95	0.7 and 12	7.03 and 7.368
[33]	28	92.2	0.445	7.88
[34]	28	95	0.85	2.2
[35]	28 and 38	-	18 — Wideband	Max Gain 13.98
[36]	28 and 38	87.5 and 91.3	1.23 and 1.06	6.6 and 5.86
proposed design	28 and 38	93.6 and 93.4	16.5 — Wideband	15.2 and 11.94

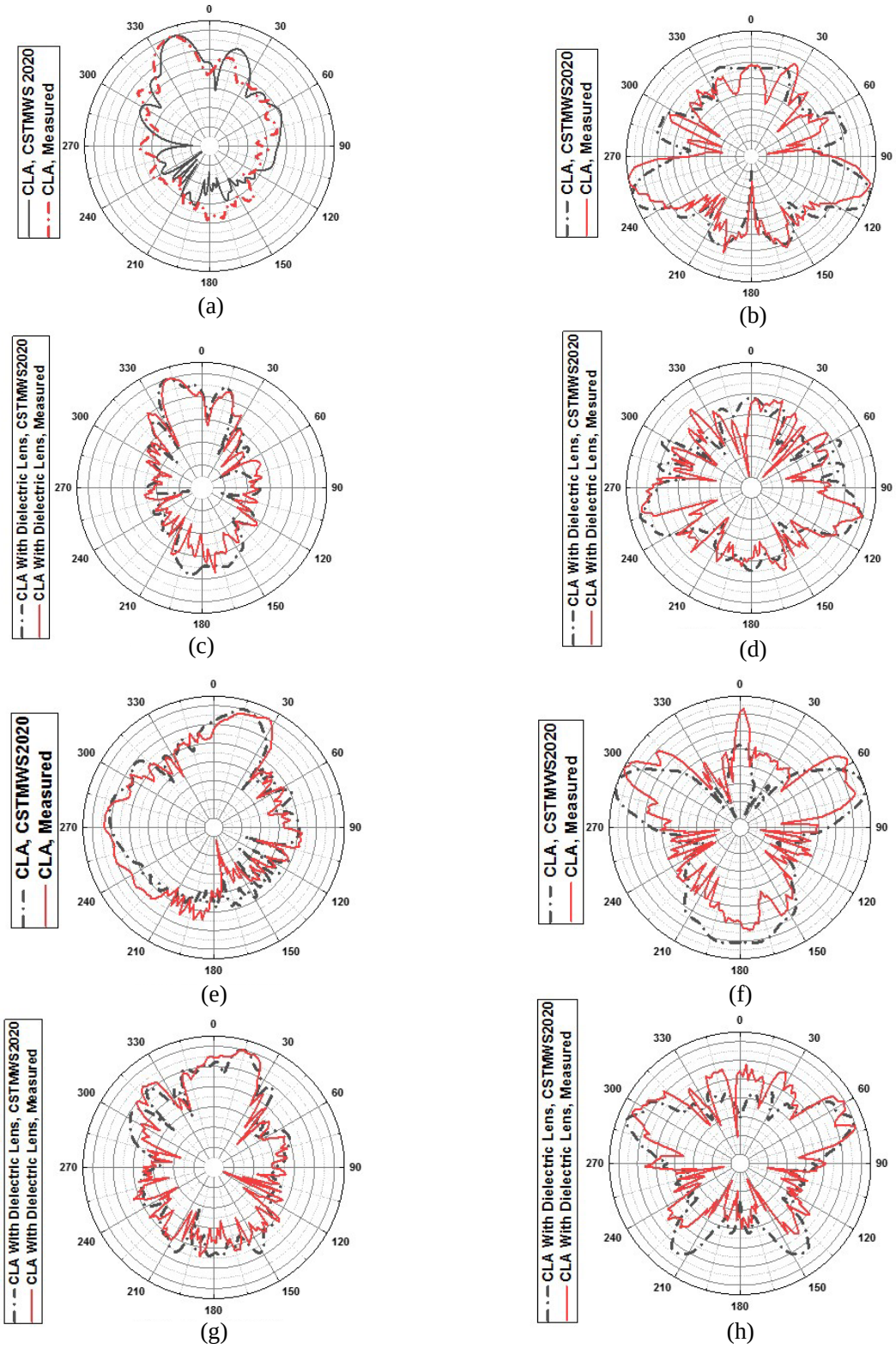

Figure 12. The 2D normalized radiation patterns of the CLA and the CLA integrated with the dielectrict lens (Type 2). (a) E-plane (28 GHz), (b) H-plane (28 GHz), (c) E-plane (28 GHz), (d) H-plane (28 GHz), (e) E-plane (38 GHz), (f) H-plane (38 GHz), (g) E-plane (38 GHz), (h) H-plane (38 GHz).

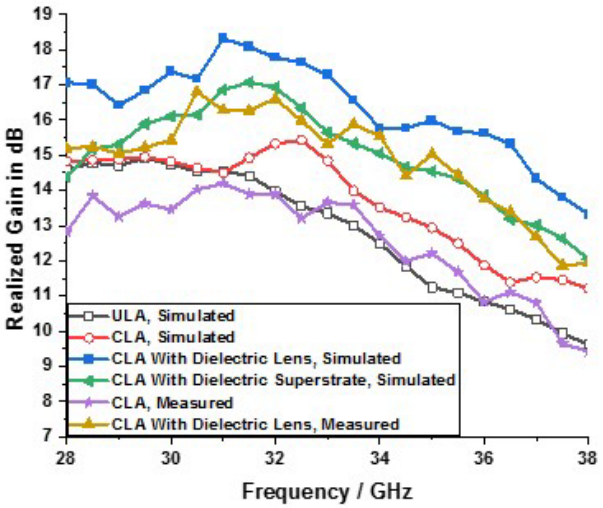

Figure 13. The realized gain versus frequency.

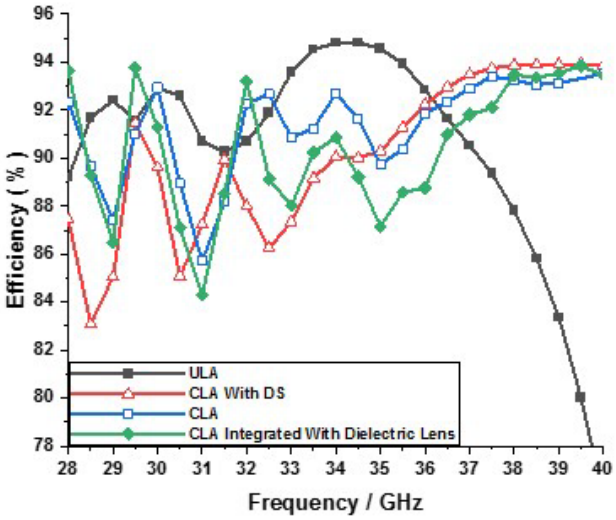

Figure 14. The total efficiency versus frequency.

The dielectric lens enhances the total efficiency of the antenna, as shown in Figure 14. Also, the realized gain is enhanced, and the realized gain versus frequency of all designed antennas is shown in Figure 13.

The proposed CLA integrated with a dielectric lens achieves high realized gain at dual-band (28/38 GHz) frequency, which reaches 15.2 and 11.94 dB, respectively.

The dielectric lens is optimized to operate mainly at 28 GHz and 38 GHz to increase radiation and the total efficiency of the proposed CLA. The total efficiencies are 93.6 and 93.4 at 28 GHz and 38 GHz, respectively.

The experimental measurement of return loss $|S_{11}|$ of the proposed CLA and CLA integrated with dielectric lens (Type 2) using VNA Rhode and Schwartz model ZVA67 is shown in Figure 15.

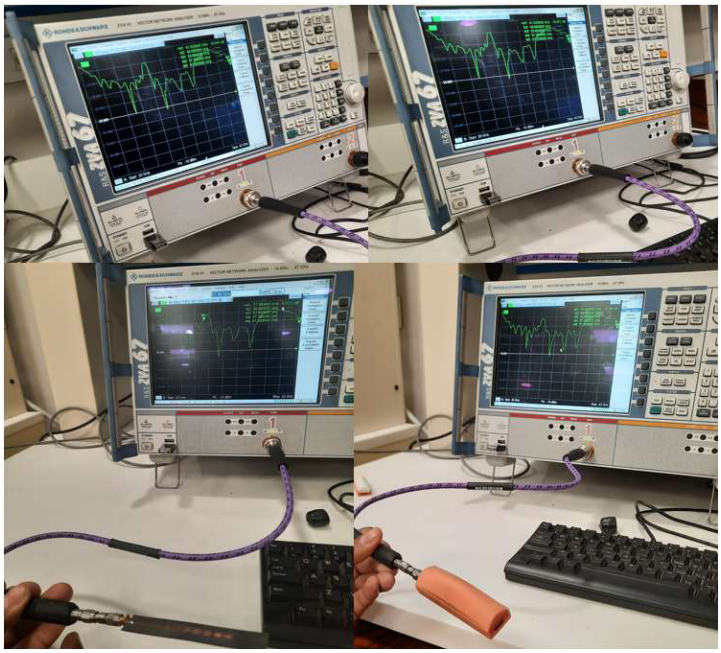

Figure 15. The experimental measurement of fabricated circuits (CLA and CLA integrated with dielectric lens Type 2) using VNA Rhode and Schwartz model ZVA67.

The dielectric lens has a light weight, small size, and makes essential differences, which increase realized gain and reduce SLL of antenna arrays over all the mentioned types of antennas. The dielectric lens is suitable for antennas that operate at high frequencies because of its size.

5. CONCLUSION

In this paper, the CLA integrated with a dielectric lens results in a significant improvement in the realized gain as well as a decrease in the SLL, which leads to an improvement in the radiation efficiency of the proposed array. Also, the study presents the surface and shape of dielectric lenses and their effects on the antenna properties, such as realized gain and efficiency. The proposed Type 2 dielectric lens is a special case of DS, which consists of dielectric parabolic and elliptical air cavities. The dielectric lens is suitable for 5G high frequency applications and can play an important role in increasing realized gain in addition to the beamforming technique. The CLA, which uses the CAD method, is better than the ULA. The proposed CLA integrated with Type 2 dielectric lens achieved a realized gain of 15.2 dB at 28 GHz and 11.94 dB at 38 GHz. 3D printing is a new technology that is rapidly gaining momentum and can be used in the fabrication of lenses to improve the realized gain, efficiency, reduce SLL, and enhance the radiation characteristics of antennas. The proposed design is introduced for 5G automotive applications to work efficiently in critical conditions and cover automotive services that are essential such as GPS, maps, driver assistance systems, and automated driving of vehicles.

REFERENCES

1. Storck, C. R. and F. Duarte-Figueiredo, "A survey of 5G technology evolution, standards, and infrastructure associated with vehicle-to-everything communications by internet of vehicles," *IEEE Access*, Vol. 8, 117593–117614, 2020.
2. Rabinovich, V. and N. Alexandrov, *Antenna Arrays and Automotive Applications*, Springer Science & Business Media, 2012.
3. Hastürkoğlu, S. and S. Lindenmeier, "A wideband automotive antenna for actual and future mobile communication 5G/LTE/WLAN with low profile," *2017 11th European Conference on Antennas and Propagation (EUCAP)*, 602–605, IEEE, 2017.
4. Pirinen, P., "A brief overview of 5G research activities," *1st International Conference on 5G for Ubiquitous Connectivity*, 17–22, IEEE, 2014.
5. Barba, M., "A high-isolation, wideband and dual-linear polarization patch antenna," *IEEE Transactions on Antennas and Propagation*, Vol. 56, No. 5, 1472–1476, 2008.
6. El-Din, M. S., S. I. Shams, A. Allam, M. F. A. Sree, A. Gaafar, and H. El-Hennawy, "Bow-tie slot antenna loaded with superstrate layers for 5G/6G applications," *2021 IEEE International Symposium on Antennas and Propagation and USNC-URSI Radio Science Meeting (APS/URSI)*, 1561–1562, IEEE, 2021.
7. Wei, L., et al., "Actual deviation correction based on weight improvement for 10-unit Dolph-Chebyshev array antennas," *Journal of Ambient Intelligence*, Vol. 10, No. 5, 1713–1726, 2019.
8. Chen, Z. N., D. Liu, H. Nakano, X. Qing, and T. Zwick, *Handbook of Antennas Technologies*, Springer Publishing Company, Incorporated, 2016.
9. Shahrubudin, N., L. T. Chuan, and R. Ramlan, "An overview on 3D printing technology: Technological, materials, and applications," *Procedia Manufacturing*, Vol. 35, 1286–1296, 2019.
10. Low, Z.-X., Y. T. Chua, B. M. Ray, D. Mattia, I. S. Metcalfe, and D. A. Patterson, "Perspective on 3D printing of separation membranes and comparison to related unconventional fabrication techniques," *Journal of Membrane Science*, Vol. 523, 596–613, 2017.
11. Stansbury, J. W. and M. J. Idacavage, "3D printing with polymers: Challenges among expanding options and opportunities," *Dental Materials*, Vol. 32, No. 1, 54–64, 2016.
12. Shahrubudin, N., T. C. Lee, and R. J. P. M. Ramlan, "An overview on 3D printing technology: Technological, materials, and applications," *Procedia Manufacturing*, Vol. 35, 1286–1296, 2019.

13. Kothapudi, V. K. and V. Kumar, "SFCFOS uniform and Chebyshev amplitude distribution linear array antenna for K-band applications," *Journal of Electromagnetic Engineering Science*, Vol. 19, No. 1, 64–70, 2019.
14. Balanis, C. A., *Antenna Theory: Analysis and Design*, John Wiley & Sons, Inc., 2015.
15. Shafai, L., *Dielectric Loaded Antennas*, John Wiley & Sons, Inc., www.researchgate.net/publication, 2005.
16. Thornton, J. and K.-C. Huang, *Modern Lens Antennas for Communications Engineering*, John Wiley & Sons, Inc., 2013.
17. Fernandes, C. A., E. B. Lima, and J. R. Costa, "Dielectric lens antennas," *Handbook of Antenna Technologies*, 1001–1064, 2016.
18. Hasan, N., N. S. M. Hussain1, A. A. M. Faudzi, et al., "Cured epoxy resin dielectric characterization based on accurate waveguide technique," *AIP Conference Proceedings*, Vol. 2129, No. 1, 020080, AIP Publishing LLC, 2019.
19. Hasan, N., N. H. Noordin, M. S. A. Karim, M. R. M. Rejab, and Q. J. Ma, "Dielectric properties of epoxy-barium titanate composite for 5 GHz microstrip antenna design," *SN Applied Sciences*, Vol. 2, No. 1, 1–8, 2020.
20. Pozar, D. M., *Microwave Engineering*, John Wiley & Sons, Inc., 2011.
21. Artemenko, A., A. Mozharovskiy, A. Maltsev, et al., "Experimental characterization of E-band two-dimensional electronically beam-steerable integrated lens antennas," *IEEE Antennas and Wireless Propagation Letters*, Vol. 12, 1188–1191, 2013.
22. Bisognin, A., D. Titz, F. Ferrero, et al., "3D printed plastic 60 GHz lens: Enabling innovative millimeter wave antenna solution and system," *2014 IEEE MTT-S International Microwave Symposium (IMS 2014)*, 1–4, IEEE, 2014.
23. Silbernagel, C. J., "Additive manufacturing 101-4: What is material jetting?" *Canada Makers*, 2018.
24. Tofail, S. A. M., E. P. Koumoulos, A. Bandyopadhyay, S. Bose, L. O'Donoghue, and C. Charitidis, "Additive manufacturing: Scientific and technological challenges, market uptake and opportunities," *Materials Today*, Vol. 21, No. 1, 22–37, 2018.
25. Lin, C.-H., Y.-M. Lin, Y.-L. Lai, and S.-Y. Lee, "Mechanical properties, accuracy, and cytotoxicity of UV-polymerized 3D printing resins composed of Bis-EMA, UDMA, and TEGDMA," *The Journal of Prosthetic Dentistry*, Vol. 123, No. 2, 349–354, 2020.
26. Belen, M. A., "Stacked microstrip patch antenna design for ISM band applications with 3D-printing technology," *Microwave Optical Technology Letters*, Vol. 61, No. 3, 709–712, 2019.
27. Zhang, Y.-X., Y.-C. Jiao, and S.-B. Liu, "3-D-printed comb mushroom-like dielectric lens for stable gain enhancement of printed log-periodic dipole array," *IEEE Antennas and Wireless Propagation Letters*, Vol. 17, No. 11, 2099–2103, 2018.
28. Mianroodi, R. Y., H. Aliakbarian, and G. A. Vandenbosch, "Dual-port dual-band (28/38 GHz) SIW leaky wave antenna for 5G base stations," *12th European Conference on Antennas and Propagation (EuCAP 2018)*, 1–4, IET, 2018.
29. Ahmad, W. and W. T. Khan, "Small form factor dual band (28/38 GHz) PIFA antenna for 5G applications," *2017 IEEE MTT-S International Conference on Microwaves for Intelligent Mobility (ICMIM)*, 21–24, IEEE, 2017.
30. Aliakbari, H., A. Abdipour, R. Mirzavand, A. Costanzo, and P. Mousavi, "A single feed dual-band circularly polarized millimeter-wave antenna for 5G communication," *2016 10th European Conference on Antennas and Propagation (EuCAP)*, 1–5, IEEE, 2016.
31. Ullah, H., F. A. Tahir, and Z. Ahmad, "A dual-band hexagon monopole antenna for 28 and 38 GHz millimeter-wave communications," *2018 IEEE International Symposium on Antennas and Propagation & USNC/URSI National Radio Science Meeting*, 1215–1216, IEEE, 2018.
32. Alnemr, F., M. F. Ahmed, and A. A. Shaalan, "A compact 28/38 GHz MIMO circularly polarized antenna for 5G applications," *Journal of Infrared, Millimeter, Terahertz Waves*, Vol. 42, No. 3, 338–355, 2021.

33. Ahmad, I., S. Houjun, Q. Ali, and A. Samad, "Design of umbrella shape single element patch antenna with high gain and high efficiency for 5G wireless communication in 28 GHz," *2020 17th International Bhurban Conference on Applied Sciences and Technology (IBCAST)*, 710–713, IEEE, 2020.
34. Lin, W., R. W. Ziolkowski, and T. C. Baum, "28 GHz compact omnidirectional circularly polarized antenna for device-to-device communications in the future 5G systems," *IEEE Transactions on Antennas and Propagation*, Vol. 65, No. 12, 6904–6914, 2017.
35. Ibrahim, I. M., M. I. Ahmed, H. M. Abdelkader, and M. J. Elsherbini, "A novel compact high gain wide-band log periodic dipole array antenna for wireless communication systems," *Journal of Infrared, Millimeter, Terahertz Waves*, 1–23, 2022.
36. Farahat, A. E. and K. F. A. Hussein, "Dual-band (28/38 GHz) wideband MIMO antenna for 5G mobile applications," *IEEE Access*, Vol. 10, 32213–32223, 2022.